ACS OMEGA

http://pubs.acs.org/journal/acsodf

Article

Optimization of Arsenic Removal from Aqueous Solutions Using Amidoxime Resin Hosted by Mesoporous Silica

Doina Humelnicu, Maria Ignat, Maria Valentina Dinu, and Ecaterina Stela Dragan*

Cite This: *ACS Omega* 2022, 7, 31069−31080

Read Online

ACCESS | Metrics & More | Article Recommendations | Supporting Information

ABSTRACT: The paper reports on the performances of cross-linked amidoxime hosted into mesoporous silica (AMOX) in the removal of As(III) and As(V). The optimum pH for sorption of As(III) and As(V) was pH 8 and pH 5, respectively. The PFO kinetic model and the Sips isotherm fitted the best the experimental data. The thermodynamic parameters were evaluated using the equilibrium constant values given by the Sips isotherm at different temperatures and found that the adsorption process of As(III) and As(V) was spontaneous and endothermic on all AMOX sorbents. The spent AMOX sorbents could be easily regenerated with 0.2 mol/L HCl solution and reused up to five sorption/desorption cycles with an average decrease of the adsorption capacity of 18%. The adverse effect of the co-existing inorganic anions on the adsorption of As(III) and As(V) onto the sorbent with the highest sorption capacity (AMOX3) was arranged in the following order: $H_2PO_4^-$ > HCO_3^- > NO_3^- > SO_4^{2-}.

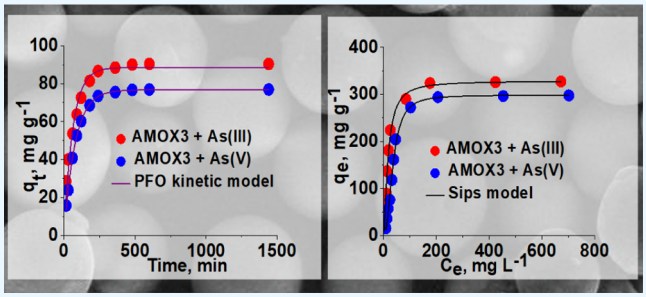

1. INTRODUCTION

Arsenic is one of the most harmful pollutants present in the surface water and groundwater as a side effect of the ore exploitation, activity of volcanoes, and some anthropogenic sources such as mining.[1−4] Industrial wastewaters containing arsenic are generated by the metallurgical industry, glassware and ceramic production, tannery operation, dyestuff and pigments manufacture, wood preservatives, and pesticide manufacturing, petroleum refining, and rare-earth industries.[5,6] Ingestion of contaminated drinking water can cause gastrointestinal damage, cardiovascular and endocrine disorders, skin cancer, and kidney cancer.[6,7] To protect the human health, the World Health Organization decreased the maximum concentration of arsenic in drinking water to 10 μg/L.[8] Arsenic exists mostly in two inorganic forms as H_3AsO_3 and H_3AsO_4, with the dominant arsenic species in groundwater being As(III), which is 60 times more toxic than As(V).[9] Therefore, there is a stringent need to develop highly efficient technologies to remove arsenic species from groundwater and wastewaters. Removal of arsenic ions is usually performed by nanofiltration and reverse osmosis,[10] electrocoagulation,[11] chemical precipitation,[12] ion exchange,[8,13−17] and adsorption.[2,7,9,18−23] Among the most accessed technologies for removal of arsenic, adsorption is obviously the most attractive by its accessible costs, easy operation, and large potential for the development of new generations of adsorbents.[9,18−23]

Various silica-based composites with good performances in the removal of heavy metal ions, or oxyanions, have been lately reported.[24−28] Among them, selective and efficient adsorption of arsenic ions by the amino-functionalized silica,[24,25] surface-ion imprinted silica,[26] or quaternary amine-functionalized silica[28] have been reported in the last decade. Porous silica has been used as a suitable host for numerous functional polymers, such as anionic hydrogels,[29] anion exchangers,[30] and amidoxime ligands.[31,32] Amidoxime-based sorbents demonstrated high potential in the removal of heavy metal ions,[32,33] or radionuclides.[31,34] However, the possibility of using sorbents containing amidoxime functional groups in the reversible adsorption of arsenic from water has not been sufficiently explored.[35] This lack of information prompted us to prepare and characterize some composites consisting of amidoxime resin entrapped into the pores of a commercial mesoporous silica and to demonstrate their performances in the removal of As(III) and As(V) as a function of the amidoxime content and textural characteristics of the composites. The effect of various adsorption parameters, such as pH, contact duration, the initial concentration of arsenic, temperature, and the presence of competitive anions on the sorption capacity, was deeply investigated by changing one parameter at a time, keeping the others constant. At the time of writing the paper, no information about the sorption performances of silica/amidoxime composites toward As(III) and As(V) has been reported.

Received: May 20, 2022
Accepted: August 11, 2022
Published: August 23, 2022

https://doi.org/10.1021/acsomega.2c03140
ACS Omega 2022, 7, 31069−31080

2. MATERIALS AND METHODS

2.1. Chemical Reagents. Mesoporous silica having textural characteristics of specific surface area, S_{sp} = 95 m^2/g; pore volume, V_p = 1.02 cm^3/g; and average pore radius, r_p = 26.7 nm was purchased from Daiso Co. (Osaka, Japan). Acrylonitrile (AN), ethyleneglycol dimethacrylate (EGDMA), azoisobutyronitrile (AIBN) (recrystallized three times from methanol), and *N*,*N*-dimethylformamide (DMF) were purchased from Sigma-Aldrich Chemie (GmbH, Germany). Toluene, methanol, NaOH, and hydroxylamine hydrochloride (HA) were purchased from Chemical Company (Romania) and used as received. $NaAsO_2$ (≥90%) and $Na_2HAsO_4{\cdot}7H_2O$ (≥98%) were purchased from Sigma-Aldrich and used as received. $NaHCO_3$, $NaNO_3$, and Na_2SO_4 were purchased from Chemical Company, and KH_2PO_4 was purchased from Fluka and used as received.

2.2. Preparation of Silica/Amidoxime Composites. The synthesis of silica/amidoxime composites was performed as previously described[31] with some changes. Cross-linked poly(acrylonitrile) (PAN) embedded into the silica pores was prepared using AIBN as an initiator (1 wt % vs monomers) and EGDMA as a cross-linker (10 wt % vs monomers), with toluene as a porogen at a ratio of 1:1 to the volume of monomers. After the adsorption of the monomer mixture into the silica pores, the polymerization was conducted 2 h at 60 °C, 3 h at 70 °C, and 7 h at 85 °C. The PAN homopolymer and toluene were removed by extraction with DMF and finally with methanol. Three PAN/silica samples were prepared in this work: SiO_2/PAN22, containing 22 wt % PAN, SiO_2/PAN15, containing 15 wt % PAN, and SiO_2/IPN, which represents the composite having two networks of PAN (homo-IPN) constructed in a sequential manner, with PAN15 as the first network.[36] The synthesis of silica/amidoxime (AMOX) from silica/PAN composites was performed by the reaction of the nitrile groups in PAN with HA as follows: 40 mL of methanolic solution of HA solution with a concentration of about 15% was added to 5 g of silica/PAN composite, the reaction being conducted at 70 °C, 5 h. The codes of the composites are as follows: AMOX1 resulted from SiO_2/PAN22; AMOX2 from SiO_2/PAN15; and AMOX3 from SiO_2/IPN.

2.3. Characterization of Silica/Amidoxime Composites. The thermogravimetric curves were recorded on a STA 449F1 Jupiter device (Netzsch, Selb, Germany) in a nitrogen atmosphere (50 mL min^{-1}). The sample (20 mg) was heated in alumina crucibles at a heating rate of 10 °C min^{-1}. FTIR spectra were recorded with a Bruker Vertex FTIR spectrometer (Bruker, Ettlingen, Germany), resolution 2 cm^{-1}, in the range of 4000−400 cm^{-1} by the KBr pellet technique. The specific surface area (S_{sp}) and the pore size distribution were estimated from N_2 adsorption−desorption experiments conducted at 77 K using an Autosorb-1-MP surface area analyzer (Quantachrome Company, Boynton Beach, FL, USA). S_{sp} was determined by the Brunauer−Emmett−Teller (BET) method, whereas the Barrett−Joyner−Halenda (BJH) theory was used to evaluate the pore size distribution. The external surface and the internal morphology of the composite microspheres having amidoxime resin into the silica pores were observed by using an environmental scanning electron microscope (ESEM) type (FEI Company, Hillsboro, Oregon, USA) Quanta 200, operating at 20 kV with secondary electrons, in the low vacuum mode. Potentiometric titration was performed using a PCD-03 particle charge detector (PCD 03; Mütek GmbH, Germany) to determine the pH_{PZC} values of the composites, defined as the pH where the potential is 0 mV. It was carried out between pH ≈ 3 and ≈11 by adjusting the pH of an aqueous suspension of microparticles using 0.1 mol·L^{-1} HCl and NaOH, respectively. The determination of As was carried out on a contrAA 800, High-Resolution Continuum Source Atomic Absorption Spectrometer (Analytic Jena AG, Germany), working in a flame mode, and equipped with a Xenon short arc lamp and an echelle grating monochromator (High-Resolution Optics). The characteristic wavelength of As (193 nm) was stabilized by using an integrated neon radiator.

2.4. Batch Sorption Experiments. Batch sorption of As(III) and As(V) onto the AMOX composites was carried out using 10 mg of sorbent and 10 mL of metalloid solution. The aqueous solutions of various concentrations were prepared from a stock solution with a concentration of 1000 mg/L. The pH of the solutions was adjusted with 0.1 M HCl or 0.1 M NaOH. After shaking for a certain time, the sorbent was separated by filtering through a 0.45 μm membrane filter. The samples collected at different contact times and at equilibrium were analyzed, after the adequate dilution, in duplicate, and the mean of three readings for each sample was used for the calculation of the sorption results.

The adsorption capacity at equilibrium, q_e (mg/g), was calculated using eq 1

$$q_e = \frac{(C_0 - C_e)V}{m} \tag{1}$$

where C_o—the initial concentration of As(III) or As(V) (mg/L), C_e—the concentration of arsenic in the aqueous solution at equilibrium (mg/L), V—the volume of the aqueous solution (L), and m—the mass of the sorbent (g).

The removal efficiency (RE) was calculated using eq 2

$$\mathrm{RE} = \frac{C_0 - C_e}{C_0} \times 100 \tag{2}$$

where C_o and C_e have the same meaning as in eq 1.

The evaluation of kinetics and isotherm parameters was performed by a nonlinear regression method using two error functions to assess the level of fit: the correlation coefficient of determination (R^2) and the nonlinear Chi-square (χ^2) test, calculated by eq 3

$$\chi^2 = \sum \frac{(q_{e,exp} - q_{e,cal})^2}{q_{e,cal}} \tag{3}$$

where $q_{e,exp}$ and $q_{e,cal}$ represent the experimental data (mg/g) and the data calculated by models (mg/g), respectively.

All experiments were repeated three times, and the data were reported as the average of three independent measurements.

2.5. Reusability. To assess the sorbent recyclability, 10 mg of sorbent and 10 mL of metal ion solution with a concentration of 100 mg/L were stirred 8 h at 22 °C at pH 5.0 for As(V) and pH 8.0 for As(III). After that, the arsenic species loaded onto the composite sorbents were eluted with 0.2 M HCl aqueous solution (20 mL) for 8 h, washed several times with distilled water, and then regenerated with 0.1 M NaOH aqueous solution (20 mL) for 6 h. After washing with distilled water, the sorbents were reused in another cycle of sorption.

2.6. Effect of Competitive Ions. For the investigation of the effect of co-existing anions on the sorption capacity of the sorbents, the following anions were considered: NO_3^-, HCO_3^-, $H_2PO_4^-$, and SO_4^{2-}. The concentration of arsenic ions was 100

https://doi.org/10.1021/acsomega.2c03140
ACS Omega 2022, 7, 31069−31080

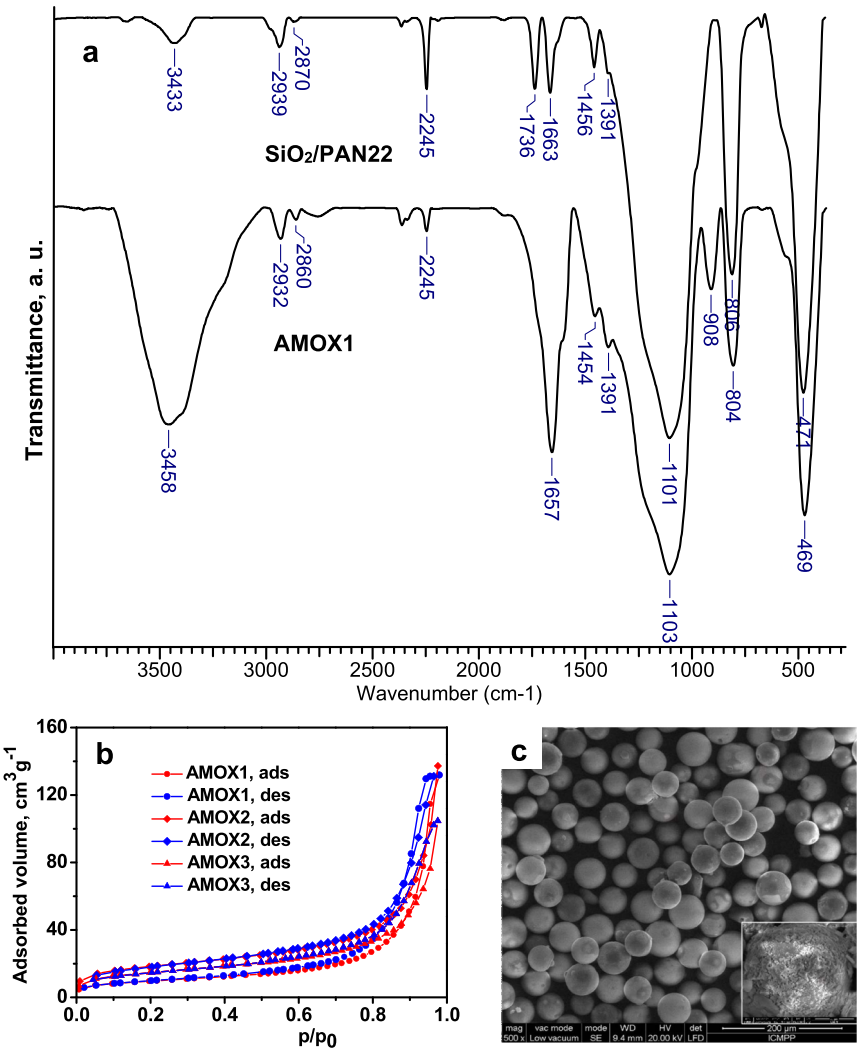

Figure 1. Characterization of AMOX composite sorbents: (a) FTIR spectra of SiO_2/PAN22 and of the AMOX1 sorbent; (b) BET isotherm of AMOX composites; and (c) SEM image of the AMOX1 sorbent; mag 500× (the inset image shows the interior morphology of AMOX1; mag. 5000×).

mg/L and that of the competing anions was 10^{-3}, 10^{-2}, and 10^{-1} M, and the ratio between the concentration of competing anions and arsenic species increased from 1 mM co-ion: 1.33 mM As up to 100 mM co-ion: 1.33 mM As.

3. RESULTS AND DISCUSSION

3.1. Characterization of AMOX Sorbents. The effective amount of organic part immobilized into silica pores after the amidoximation of the nitrile groups was determined by TGA. As can be seen in Figure S1, all AMOX composite sorbents displayed a thermal degradation pattern in four stages. The first stage corresponds to loss of physically absorbed water and other residual traces, summing up 2.51, 1.54, and 1.52% for AMOX1, AMOX2, and AMOX3, respectively. In the second stage of thermal degradation, the mass loss values were 7.17, 3.9, and 4.76% for the same order of the composites. The main thermal degradation stages were the third and fourth, occurring above 253.24, 242.24, and 241.87 °C for AMOX1, AMOX2, and AMOX3, respectively. The total percentage of weight loss in the third and fourth stages, up to 700 °C, was 20.35% for AMOX1, 14.15% for AMOX2, and 17.34% for AMOX3. These thermal degradation stages are associated with the disruption of cross-links between the main chains and main chain degradation.

Figure 1a presents the FTIR spectra of the composite SiO_2/PAN22 and of the composite AMOX1 resulted by the transformation of the nitrile groups in amidoxime. This pair of composites was taken as an example, the main bands being present in the other samples of SiO_2/PAN and AMOX.

The characteristic bands of PAN are visible at 2928 and 2860 cm^{-1} attributed to the stretching vibrations of $-CH_3$ and methylene groups in PAN cross-linked with EGDMA; the band located at 2245 cm^{-1} is characteristic to the stretching of the $-C\equiv N$ groups; the band at 1736 cm^{-1} was assigned to the $C=O$ groups in the ester groups of EGDMA used as a cross-linker; the band at 1456 cm^{-1} was attributed to the stretching vibrations of $-CH_2$- groups, while the band of medium intensity situated at 1391 cm^{-1} was assigned to the symmetrical deformation mode in CH_2 and CH_3 groups.[37] The large band at 1101 cm^{-1} and the sharp bands located at 806 and 471 cm^{-1} were assigned to the stretching vibration of Si−O−Si bonds, to the bending vibrations of Si−O bonds, and to the out-of-plane vibrations of Si−O bonds, respectively. After amidoximation, the main bands visible in the spectrum of AMOX1 are as follows: 2932 and 2860 cm^{-1} attributed to the stretching vibrations of $-CH_3$ and methylene groups; a small peak at 2245 cm^{-1}, which shows that some residual $-C\equiv N$ groups are still present in the composite; the large band situated at 1657 cm^{-1}, which screen

https://doi.org/10.1021/acsomega.2c03140
ACS Omega 2022, 7, 31069−31080

the stretching vibration band of the C═O groups, was assigned to the amidoxime groups; the small peak at 1454 cm^{-1} was attributed to the stretching vibrations of $-CH_2-$ groups, while the band of medium intensity situated at 1391 cm^{-1} was assigned to the symmetrical deformation mode in CH_2 and CH_3 groups. The characteristic bands of silica are located at 1103, 804, and 469 cm^{-1}.

It was demonstrated that the adsorption of various ions in an aqueous solution was influenced by the textural characteristics of the sorbent.[38] The representative plots of BET isotherms for AMOX composites are presented in Figure 1b. As can be seen, all isotherms correspond to type IV, as categorized by the IUPAC classification, indicating the uniformity and regularity of the textural properties of all composites. The textural parameters, evaluated based on the isotherms in Figure 1b, are summarized in Table 1.

Table 1. Specific Surface Area and Pore Volume of the AMOX Composites Evaluated by the BET Method

sample code	Ssp, m^2/g	Vp, cm^3/g,	R^2
AMOX1	34.00	0.178, pores with d < 44.8 nm	0.9998
AMOX2	64.06	0.158, for pores with d < 46.8 nm	0.9998
AMOX3	51.31	0.118, for pores with d < 44.7 nm	0.9996

As can be seen in Table 1, the BET surface area of the AMOX composites, calculated by applying the BET equation to the linear part ($0.05 < P/P_0 < 0.305$) of the adsorption isotherm, is 34, 64.06, and 51.31 m^2/g for AMOX1, AMOX2, and AMOX3, respectively. It is obvious that the specific surface area of the AMOX composites is much lower than that of the pristine mesoporous silica (S_{sp} = 95 m^2/g), all the more so as a higher amount of amidoxime resin was embedded into the silica pores (AMOX1 compared with AMOX2). Also, the construction of the second network of PAN, which after the amidoximation conducted to the second network of amidoxime, is associated with the decrease of the specific surface area (AMOX3 compared with AMOX2). The majority of pores are located in the range of 5−20 nm, indicating that all composites have a mesoporous structure as can be seen from the pore size distribution profiles (Figure S2). The external surface of the composite microspheres is visible in Figure 1d. The internal morphology of the composite AMOX1 can be seen in the inset of Figure 1d.

3.2. Arsenic Removal in the Batch Mode. *3.2.1. Effect of pH.* The adsorption of arsenic is expected to be strongly influenced by the solution pH due to the different anionic species, which could be generated when the pH changes. The effect of the initial solution pH on the adsorption of As(III) and As(V) onto AMOX composites is presented in Figure 2a.

As can be seen, the optimum initial pH value for the removal of As(V) from aqueous solution was 5.0 while for As(III) was 8.0. At pH lower than 2.24, only nondissociated molecules of H_3AsO_4 are present in solution.[9,15,39−41] Increasing the pH from 2 to 5, the adsorption of As(V) oxoanions increased and then monotonously decreased; this would indicate that at pH near to 5, there is an optimum concentration of H^+ for the adsorption of As(V) as $H_2AsO_4^-$.[7,8,40,42] It was reported that the concentration of $H_2AsO_4^-$ as dominant species increases up to pH 6.96 (pK_{a_2} for H_3AsO_4).[15,39] Yu et al.[42] have also reported the optimal pH for the removal of arsenate by cellulose-*g*-glycidyl methacrylate-*b*-tetraethylenepentamine at pH 5.0; the diminish of the As(V) adsorption at pH > 6.0 has been observed for activated carbon composites.[43] Such domain for the optimum pH for the adsorption of As(V) has been recently identified by Wei et al.[44] using as adsorbent an amine-functionalized acrylic fiber. An optimum pH in the range 6.0−7.0, for the adsorption of As(V), has been reported for aminoalkyl-organo-silane-treated sand.[45] Dudek and Kolodynska also observed the increase of As(V) adsorption with the increase of pH up to 5.0 and a steady decrease after that.[16]

Figure 2b shows that the synthesis strategy of the composite sorbent influenced the point of zero charge (PZC). Thus, the values of PZC obtained by plotting the streaming potential as a function of pH are as follows: 6.65 for AMOX1, 6.47 for AMOX3, and 6.23 for AMOX2, and indicate that the surface of all sorbents was positively charged at pH < 5.0, which was found to be optimum for the adsorption of As(V). The shape of the titration curves was similar for all sorbents, the order of PZC values being AMOX1 > AMOX3 > AMOX2. This order would indicate that the incorporation of a higher amount of PAN conducted to a composite with a higher amount of amidoxime after the amidoximation reaction (the pristine composite SiO_2/PAN for the synthesis of AMOX1 and AMOX2 sorbents was containing 22% PAN and 15% PAN, respectively). The fact that the PZC value of the sorbent AMOX3 is located in between the values corresponding to AMOX1 and AMOX2 is connected with the amount of amidoxime incorporated in silica pores, which was 20.35% for AMOX1, 14.15% for AMOX2, and 17.34% for AMOX3 (information acquired from the TG analysis, Figure S1). At pH < PZC, the negatively charged species of As(V) ions are electrostatically attracted to the protonated surface of amidoxime sorbent. Therefore, pH 5 was kept as optimum for the next sorption experiments of As(V).

Figure 2a shows that, unlike As(V), the optimum pH for the adsorption of As(III) anions was located at 8.0, where all sorbents are negatively charged. Up to pH 8, As(III) is present in water only as H_3AsO_3, the pK_{a_1} value being 9.29.[45] The decreasing trend in As(V) and increasing trend in As(III) sorption with the increase of pH value by different metal-based adsorbents has been attributed to the formation of surface species. In contrast to As(V), at high pH, As(III) is present as $H_2AsO_3^-$ ions, while at pH < 9.24, the noncharged $As(OH)_3$ is dominant, which explain the nonadsorption of As(III) at low pH.[40,43] However, at pH > 9.24, the negatively charged species of As(III) are rejected by the negatively charged surface of the sorbents. Furthermore, the RE was much higher in the case of As(III) than for As(V) and that is a very interesting characteristic of these amidoxime-based composite sorbents.

3.2.2. Effect of Contact Time. The adsorption kinetics of As(III) and As(V) onto the AMOX composites are presented in Figure 2c,d, respectively. As can be observed, the sorption of As(III) was fast and reached the equilibrium in about 3 h (Figure 2c). The adsorption of As(V) was slower and reached equilibrium in about 4 h (Figure 2d). The adsorption kinetics was carefully examined to get information about the sorption mechanism and on the rate-controlling steps of the adsorption process.[7] Some kinetics models were fitted on the experimental data, that is, pseudo-first-order (PFO),[46] pseudo-second-order (PSO),[47] and Elovich[48] models, whose equations are included in Table S1. The kinetic parameters in Table S1 show that the q_e values calculated by the PFO kinetic model were closer to those given by the experimental data. Furthermore, the coefficients of determination (R^2) were higher in the case of PFO kinetic model than in the case of PSO model, and this shows that the kinetic

https://doi.org/10.1021/acsomega.2c03140
ACS Omega 2022, 7, 31069−31080

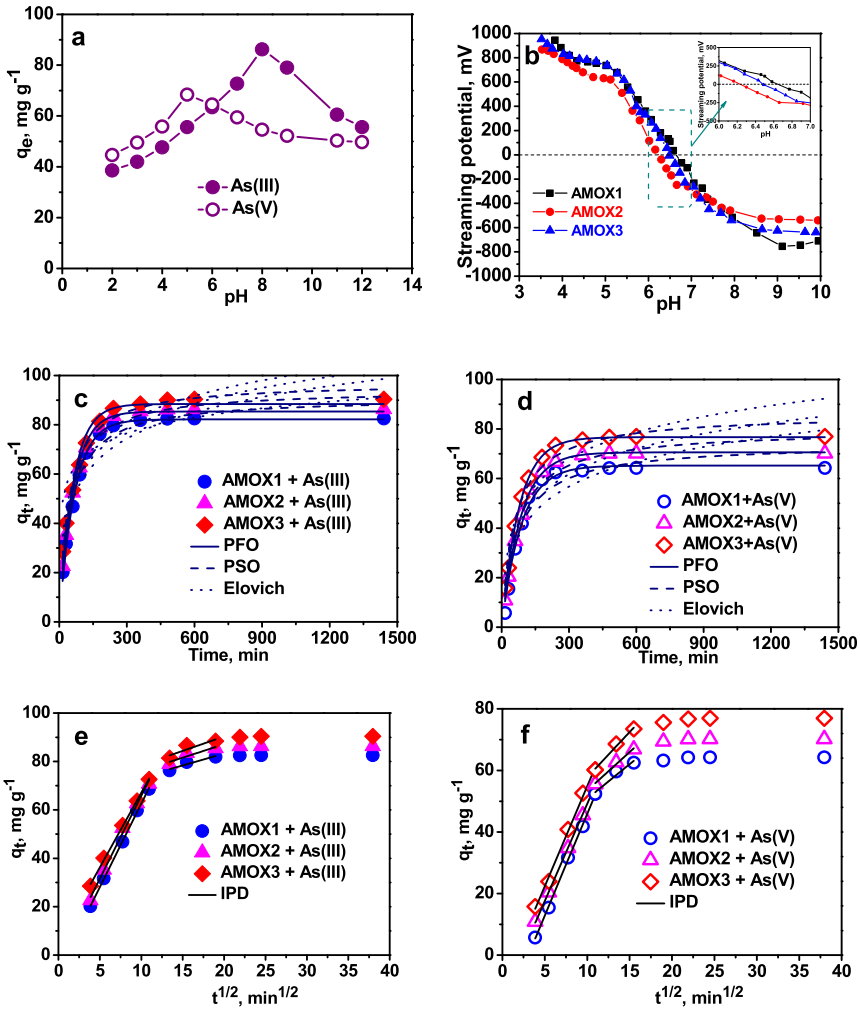

Figure 2. Effect of initial solution pH on the sorption of As(III) and As(V) oxyanions onto AMOX1 (a); streaming potential as a function of pH for the composite sorbents (b); sorption kinetics of As(III) (c) and As(V) (d) oxyanions onto AMOX sorbents fitted by PFO, PSO, and Elovich models; and IPD model fitted on the sorption of As(III) (e) and As(V) (f) oxyanions onto AMOX sorbents. Sorption conditions: sorbent dose 0.010 g; C_i = 100 mg/L; V_{sol} = 10 mL; pH = 8, for As(III), and 5 for As(V); temp. 22 °C.

process is the best described by PFO model, as found for other systems.[7,8,41]

The Elovich kinetic model reveals the role of adsorbent surface heterogeneity and supports chemisorption as the possible mechanism of sorption. However, Table S1 shows that the values of R^2 are <0.9 in the case of Elovich model, and this indicates that the adsorption mechanism of arsenic is not of the chemisorption type.[16,41]

The contribution of film diffusion and intraparticle diffusion (IPD) was clarified by fitting the IPD model.[49] The plots of q_t versus $t^{0.5}$ for the sorption of As(III) and As(V) onto the AMOX composite sorbents are presented in Figure 2e,f, respectively. It is obvious that the adsorption process is multi-stage, indicating that the IPD was not the only rate-limiting step as assessed for the adsorption of arsenic onto other sorbents.[7,24,45] The first straight line could be attributed to the diffusion of arsenic through the boundary layer (film diffusion) and the second one, with lower constants, could be assigned to the internal diffusion stage. The last step is connected to the saturation of the binding sites. The values of k_{id}, C_i, and R^2 for the first and the second steps in Figure 2e,f are presented in Table S1. The high values of R^2 for the first step ($R^2 > 0.99$) would indicate the applicability of the IPD model for the sorption of arsenic onto these composite sorbents. For the first step, the values of k_{id} are almost similar, while the values of C_i were low and increased from AMOX1 to AMOX3, being always higher for As(III) than for As(V). These results are in agreement with those obtained by fitting the PFO kinetic model and would indicate that the adsorption is more favorable on AMOX3 than on the first two sorbents. The C_i values give indication about the contribution of the boundary layer thickness, which means the larger the intercept, the greater the contribution of the film diffusion in the rate-limiting step.[31,45] The higher values of C_i reveal a larger contribution of the boundary layer in the adsorption process of As(III) than of As(V).

3.2.3. Adsorption of As(III) and As(V) at Equilibrium. By the investigation of adsorption at equilibrium, useful information is obtained, which help in the identification of the interactions between the adsorbate and the adsorbent.[39] The experimental adsorption isotherms for As(III) and As(V) are plotted in Figure 3a,b, respectively.

The experimental data of the adsorption at equilibrium were analyzed by fitting four isotherm models, Langmuir, Freundlich, Sips, and Dubinin−Radushkevich.[50−53] The isotherm equations and the obtained parameters are presented in Table 2. The Langmuir isotherm model presumes the adsorption occurs onto

https://doi.org/10.1021/acsomega.2c03140
ACS Omega 2022, 7, 31069−31080

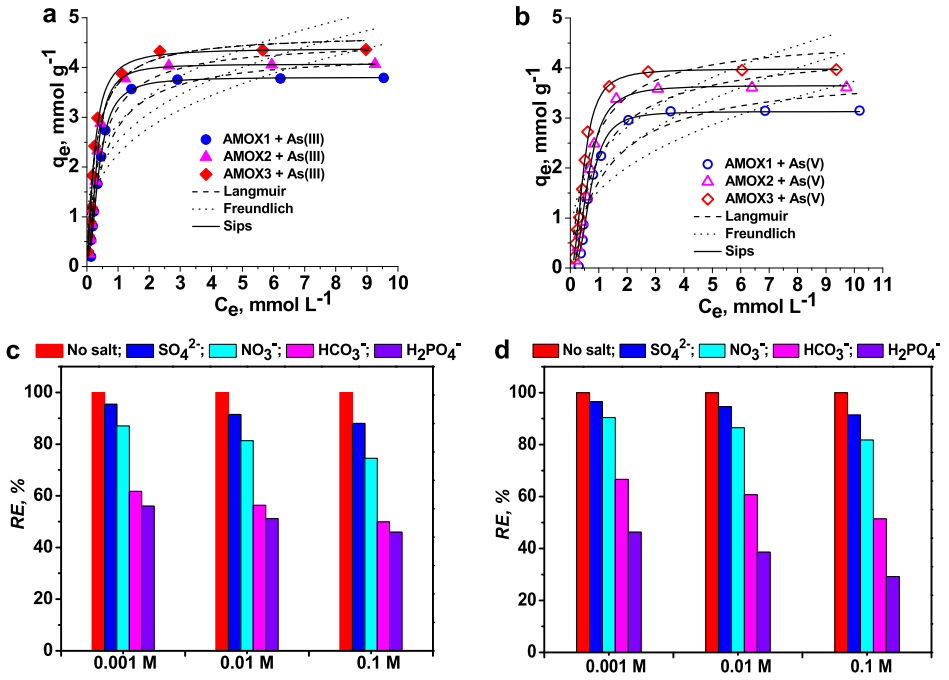

Figure 3. Sorption isotherms of As(III) (a) and As(V) (b) onto AMOX sorbents and influence of co-existing anions on the adsorption of As(III) (c) and As(V) (d) onto AMOX3 sorbent.

specific sites energetically equivalent, as a monolayer, with no interactions between the adsorbed molecules. The Freundlich isotherm is used to model the adsorption process onto heterogeneous surfaces, assuming that the binding sites are not equivalent and interactions between the adsorbed molecules are workable. This empirical model is not suitable for the experimental isotherms, which present a saturation plateau.

The Sips isotherm equation fuses the Langmuir and Freundlich isotherms in a three-parameter isotherm, suitable to model the experimental data which show a saturation plateau. As can be seen in Table 2, the highest values of R^2 and the lowest values of χ^2 were obtained for the Sips isotherm, and this indicates this isotherm as the most suitable model to describe the sorption process of As(III) and As(V) onto AMOX sorbents. Furthermore, the values of q_e were very close to the experimental values, while the Langmuir isotherm overestimated the values of q_e. These results would indicate that the sorption process of As(III) and As(V) probably occurred by multisite interactions, well described by the three-parameter isotherms such as the Sips isotherm model.[52−54] As it was expected, the Freundlich isotherm was not appropriate to describe the experimental data, the values R^2 being the lowest and those of χ^2 the highest. The favorable adsorption process is supported by the values of $1/n$ in the Freundlich isotherm, which are in the range 0−1, for all pairs AMOX sorbent/sorbate (Table 2). It would have been expected as the AMOX1 composite, having the highest content of amidoxime and the highest PZC (Figure 2b), to adsorb the highest amount of arsenic ions. However, the highest values of q_m resulted by modeling the experimental data with the Sips isotherm and with the Langmuir isotherm were obtained in the case of AMOX3 composite, both for As(III) and As(V). The enhance of q_m values could be attributed to the presence of two amidoxime networks inside the silica pores, which ensure a better accessibility of arsenic to the amidoxime groups. The specific surface area of the AMOX3 composite (Table 1) is much higher than that of AMOX1, and this difference could also contribute to the increase of the sorption performances. The values of q_m were always higher for As(III) than for As(V) (Table 2), and this fact could be associated with the adsorption of As(V) as oxoanions (ion exchange) and of As(III) by physisorption.

Information about the nature of interactions between the functional groups of sorbent and the sorbate species could be drawn by the evaluation of mean free energy of adsorption, E (kJ mol^{-1}), defined as the free energy when 1 mol of ion is transferred from infinity in solution to the surface of a solid, which is related to the Dubinin−Radushkevich isotherm constant, β, by eq 4

$$E = 1/(2\beta)^{1/2} \quad (4)$$

Recently, it was reported that to gain reliable values of the Dubinin−Radushkevich isotherm constant, the concentration term must be dimensionless, and for this reason, the term should be $(1 + C_o/C_e)$, where C_o = 1 mol L^{-1} represents the standard state of the solution, and the units of C_e must be mol L^{-1}.[55−57] Therefore, the values of β were acquired by nonlinear fitting of the Dubinin−Radushkevich isotherm on the experimental equilibrium data plotted in Figure S3 with concentration in mol/L. As can be observed in Table 2, the Dubinin−Radushkevich isotherm does not fit so well the experimental data, the R^2 values being in the range 0.8−0.86. Therefore, the values of E calculated with eq 4, by using the values of the D−R equilibrium constant (β) resulted by fitting the Dubinin−Radushkevich isotherm on the experimental data, should be considered only as an order of magnitude (Figure S3).[57] Nevertheless, the values of E in the range 10−12 kJ/mol and the fact that the kinetic data were fitted the best by the PFO kinetic model could be associated with physical sorption as the most probable mechanism for adsorption of As(III) and As(V) onto AMOX sorbents.

The sorption capacity of the AMOX3 composite against As(III) and As(V) is compared in Table 3 with the values

https://doi.org/10.1021/acsomega.2c03140
ACS Omega 2022, 7, 31069−31080

Table 2. Isotherm Parameters of Langmuir, Freundlich, Sips, and Dubinin−Radushkevich Models for the Sorption of As(III) and As(V) onto the AMOX-Type Sorbents, at 22 °C

	AMOX1		AMOX2		AMOX3	
isotherm parameters	As(III)	As(V)	As(III)	As(V)	As(III)	As(V)
Langmuir Model: $q_e = \frac{q_m K_L C_e}{1 + K_L C_e}$						
q_m, mmol g^{-1}	4.3108	3.934	4.5454	4.3926	4.68	4.6376
K_L, L $mmol^{-1}$	1.852	0.7782	2.3527	0.9878	3.6455	1.4076
R^2	0.9286	0.8571	0.9387	0.8953	0.9761	0.9155
χ^2	0.14	0.21	0.14	0.2	0.06	0.2
Freundlich Model: $q_e = K_F C_e^N$						
K_F, $mmol^{1-1/n}\cdot L^{1/n}\cdot g^{-1}$	2.2598	1.54	2.522	1.882	2.867	2.2357
$1/n$	0.302	0.3843	0.2871	0.363	0.2612	0.331
R^2	0.7309	0.6919	0.7384	0.7195	0.8023	0.7311
χ^2	0.53	0.46	0.6	0.53	0.5	0.6
Sips Model: $q_e = \frac{q_m a_S C_e^N}{1 + a_S C_e^N}$						
q_m, mmol g^{-1}	3.803	3.1287	4.068	3.6491	4.3835	3.98
a_S	7.01	2.581	10.856	2.996	9.13	5.575
$1/n$	1.997	2.846	2.011	2.464	1.484	2.302
R^2	0.9952	0.9879	0.9972	0.9971	0.9895	0.9947
χ^2	0.01	0.02	0.006	0.01	0.027	0.02
Dubinin−Radushkevich Model: $q_e = q_{DR}\exp\left\{-\beta\left[RT\ln\left(1 + \frac{C_o}{C_e}\right)\right]^2\right\}$						
q_{DR}, mol g^{-1}	0.00739	0.00767	0.00766	0.00734	0.00809	0.00826
β, $mol^2\ J^{-2}$	4.015×10^{-9}	3.734×10^{-9}	3.250×10^{-9}	5.432×10^{-9}	5.034×10^{-9}	4.458×10^{-9}
E, kJ mol^{-1}	11.16	11.57	12.4	9.59	9.97	10.59
R^2	0.7937	0.8021	0.8653	0.7952	0.8173	0.8287
χ^2	0.0001	0.0001	0.0001	0.0001	0.0001	0.0001

reported in the literature for other sorbents developed for the removal of arsenic species, along with the testing conditions.

Based on the data presented in Table 3, it can be inferred that the AMOX3 composite investigated in this work displays great potential in the removal of both As(III) and As(V). It should be pointed out that our AMOX3 composite exhibited considerably higher q_m values for the removal of As(III) than other reported materials such as calix[4]pyrrole,[13] ceramic alumina coated with chitosan,[40] iron-impregnated granular-activated carbon,[43] tetraethylenepentamine-functionalized acrylic fiber,[44] iron−chitosan composites,[58] and MWCNTs@PANI@TiO_2 nanocomposites.[60]

3.2.4. Interference with Co-existing Anions. The investigation of the influence of the co-existing anions present in water on the sorbent performances in the removal of arsenic species has a great significance for practical applications. Therefore, the influence of four co-existing anions (SO_4^{2-}, NO_3^-, HCO_3^-, and $H_2PO_4^-$), with concentrations up to 10^{-1} M, on the sorption capacity of the composite AMOX3 for As(III) and As(V), was deeply investigated. Figure 3c,d indicates an obvious decline of the adsorption capacity for arsenic, as much as the concentration of competing anions increased from 10^{-3} to 10^{-1} M, the ratio between the concentration of competing anions and arsenic species increasing from 1 mM co-ion: 1.33 mM As up to 100 mM co-ion: 1.33 mM As. By the exploration in detail of the influence of the competitive anions on the adsorption of As(III) onto the AMOX3 composite (Figure 3c), it can be observed that $H_2PO_4^-$ anions caused the highest decrease of the arsenic adsorption, the influence of HCO_3^- anions being comparable with that of $H_2PO_4^-$, similar to the results recently reported in the literature.[22,61] However, the $H_2PO_4^-$ anions could not completely inhibit the adsorption of As(III), even at a ratio of 100 mM co-ion: 1.33 mM As. The final order concerning the adverse effect of the competing anions on the adsorption of As(III), obvious in Figure 3c, is as follows: $H_2PO_4^- > HCO_3^- > NO_3^- > SO_4^{2-}$. For the adsorption of As(V) oxoanions (Figure 3d), the order was similar to that observed for As(III), but the decline in the presence of $H_2PO_4^-$ anions was more consistent. This reduction was attributed to the competition between the interfering anions ($H_2PO_4^-$) and $HAsO_4^{2-}$ for the adsorption sites of the composite sorbent. Wei et al. observed a similar order for the adsorption of As(V) oxoanions onto an amine sorbent: $PO_4^{3-} > SO_4^{2-} > NO_3^-$.[44] The highest interference observed in the case of PO_4^{3-} anions is explained by the similarity of the chemical structure of this anion with that of the arsenic anion, which, therefore, could desorb As(V) oxoanions.[61,62] It is also obvious that, for the same concentration of the competitive anions, the negative influence of HCO_3^- was less dramatic in the case of As(V) (Figure 3d) than in the case of As(III) (Figure 3c),

https://doi.org/10.1021/acsomega.2c03140
ACS Omega 2022, 7, 31069−31080

Table 3. Comparison of Maximum Equilibrium Sorption Capacity of As(III) and As(V) Ions onto Different Recently Reported Sorbents

	sorption conditions			q_m, mg/g	
sorbent	T, K	sorbent dose, g/L	initial pH	As(III)	As(V)
layered double hydroxides embedded into alginate/PVA beads[5]	303	30	8		1.73
calix[4]pyrrole[15]	298	1	6.3	14.29	15.28
hydrous TiO_2 nanoconfined in the pores of anion exchangers[21]	298	0.5	2		26.6
hydrous Fe_2O_3 nanoparticles embedded in anion exchangers[22]	298	0.5	7		31.6
chitin-g-amidoxime[35]	303	15	6.5	19.72	
ion-exchange resins containing *N*-methyl-D-glucamine[39]	303	5	6.0		237
			9.0		392
ceramic alumina coated with chitosan[40]	298	10	4	56.5	96.46
iron-impregnated granular-activated carbon[43]	298	1	4.8	98.4	125
tetraethylenepentamine-functionalized acrylic fiber[44]	293	1	7.0	40.5	270.3
silica polyamine composites[59]	298	10	4		98
			6		56
iron−chitosan composites[58]	298	5	7	16.15	22.47
MWCNTs@PANI@TiO_2 nanocomposites[60]	298	5	5	57.37	
amidoxime resin hosted by mesoporous silica (AMOX3) (this work)	295	1	8	328.7	
			5		298.6

while the decline in the adsorption of As(V) oxoanions was more dramatic when $H_2PO_4^-$ was the competitive anion.[63] The adverse effect of HCO_3^- anions was also associated with the probability as these anions to form inner-sphere complexes similar to $H_2PO_4^-$.[61] The decline of the adsorption capacity of AMOX3 for both As(III) and As(V), in the presence of SO_4^{2-} and NO_3^- anions, was not so dramatic, probably because these anions could be only bound by outer-sphere complexation.[22,61,63,64]

3.2.5. Structural Changes after Arsenic Adsorption. Information about the structural changes of the AMOX composites after the sorption of As(III) and As(V) was obtained by the analysis of the FTIR spectra of the sorbents loaded with arsenic (Figure 4) (the AMOX3 sorbent was taken as an example).

The characteristic bands arising from the stretching vibration of the As−O bond are present at 899 cm^{-1}, for AMOX3+As(V), and at 883 cm^{-1} for AMOX3+As(III) as previously reported.[8,44,65] The bands at 899 cm^{-1} in the FTIR spectra of AMOX3, after the adsorption of arsenate, would indicate the stretching frequencies of As−O bands in the $H_2AsO_4^-$ group.[58]

3.2.6. Thermodynamics. Because the Sips isotherm fitted the best the experimental equilibrium data, the equilibrium constants obtained by fitting the Sips model onto the experimental isotherms, with concentrations expressed in mmol L^{-1}, at four temperatures (295, 303, 313, and 323 K, Figure 5a,b,c), were considered as the thermodynamic equilibrium constants and were used to evaluate the change of the Gibbs free energy (ΔG^0, kJ mol^{-1}) according to eq 5

$$\Delta G^o = -RT \ln K^o \quad (5)$$

where T—the absolute temperature (K) and R—the universal gas constant (8.314 J mol^{-1} K^{-1}).

The units of K^o resulted by the nonlinear fitting of the Sips isotherm are L $mmol^{-1}$. To transform K^o in a dimensionless parameter, eq 6 was used[57,66]

$$K^o = \frac{K_{Sips} \times 10^3 \times C^o_{As}}{\gamma_{As}} \quad (6)$$

where K_{Sips} is the equilibrium constant given by the model (Sips isotherm, L $mmol^{-1}$, transformed in L mol^{-1} by multiplying with 10^3), $C_{As}{}^o$ (mol L^{-1}) is the standard concentration of As(III) or As(V), and γ_{As} (dimensionless) is the activity coefficient of As(III) and As(V) (~1, in dilute solutions).

The evaluation of the enthalpy change, ΔH^o (kJ mol^{-1}), and the entropy change, ΔS^o (J mol^{-1} K^{-1}), was carried out by using the Van't Hoff equation (eq 7), plotted in Figure 5d

$$\ln K^o = \frac{\Delta S^o}{R} - \frac{\Delta H^o}{RT} \quad (7)$$

The calculated values of the thermodynamic parameters for As(III) and As(V) adsorption onto the three sorbents are given in Tables 4 and 5, respectively.

The positive values of the enthalpy change ($\Delta H°$) demonstrate that the process of As(III) and As(V) adsorption onto the sorbents is endothermic. The positive values of the entropy change ($\Delta S°$) suggested an increase in disorder at the solid/solution interface during the arsenic adsorption process. The negative values of the Gibbs free energy (ΔG^o) observed at all temperatures indicate that the adsorption process of both As(III) and As(V) onto the three sorbents was spontaneous and favorable. The increase of the negative values of ΔG^0 with the increase of temperature indicates the increase of the degree of spontaneity of adsorption process.

3.2.7. Reusability. The adsorption performances of a sorbent toward solutes also refer to the regeneration and reuse in as many as possible successive sorption/desorption cycles.[5,37,41,53] A suitable desorption process should be used to re-establish the sorption capacity close to the initial performances.[37] Because arsenic acid is a weak acid, when acid reagents are used as eluents, the arsenic monovalent and divalent anions attached to the resin ($H_2AsO_4^-$ and $HAsO_4^{2-}$) are transformed into the noncharged molecule of H_3AsO_4, which can be leached from the sorbent.[40,41] Regeneration of the AMOX sorbents with 0.1 M NaOH proved to be a convenient way to recuperate the sorption abilities of AMOX sorbents.

As Figure 6a shows, the RE values for the sorption of As(III) onto AMOX1, AMOX2, and AMOX3 sorbents decreased from 83.22, 85.61, and 89.46%, in the first cycle, down to 65.82, 67.29, and 71.84%, in the fifth cycle, respectively. The removal of As(V) by AMOX1, AMOX2, and AMOX3 was found to be 65.37, 69.42, and 76.19% in the first cycle and decreased down to 47.59, 48.18, and 58.36% in the fifth cycle, respectively (Figure 6b).

The *RE* values decreased with about 18% from the first to the fifth cycle, and this shows that the AMOX sorbents could be regenerated and reused in the arsenic removal in multiple cycles. The same sequence of eluent and regeneration agent (0.2 M HCl and 0.1 M NaOH) proved to be effective for other sorbents.[41] These results clearly demonstrate promising possibilities for practical application of the AMOX sorbents owing to their effective arsenate removal.

https://doi.org/10.1021/acsomega.2c03140
ACS Omega 2022, 7, 31069−31080

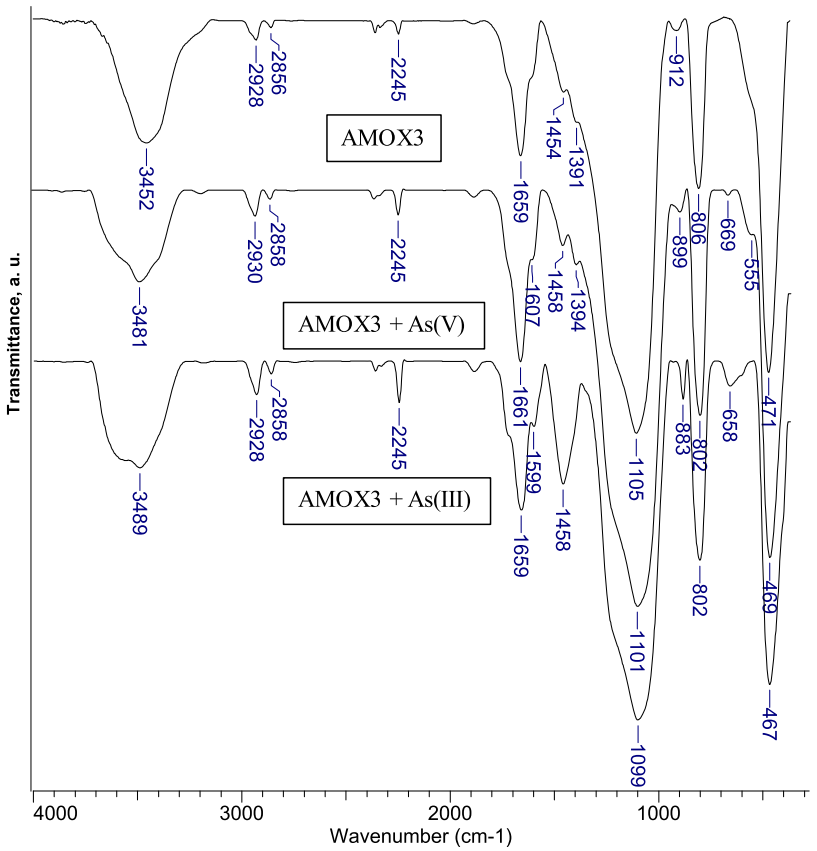

Figure 4. FTIR spectra of the AMOX sorbent before and after loading with As(III) and As(V).

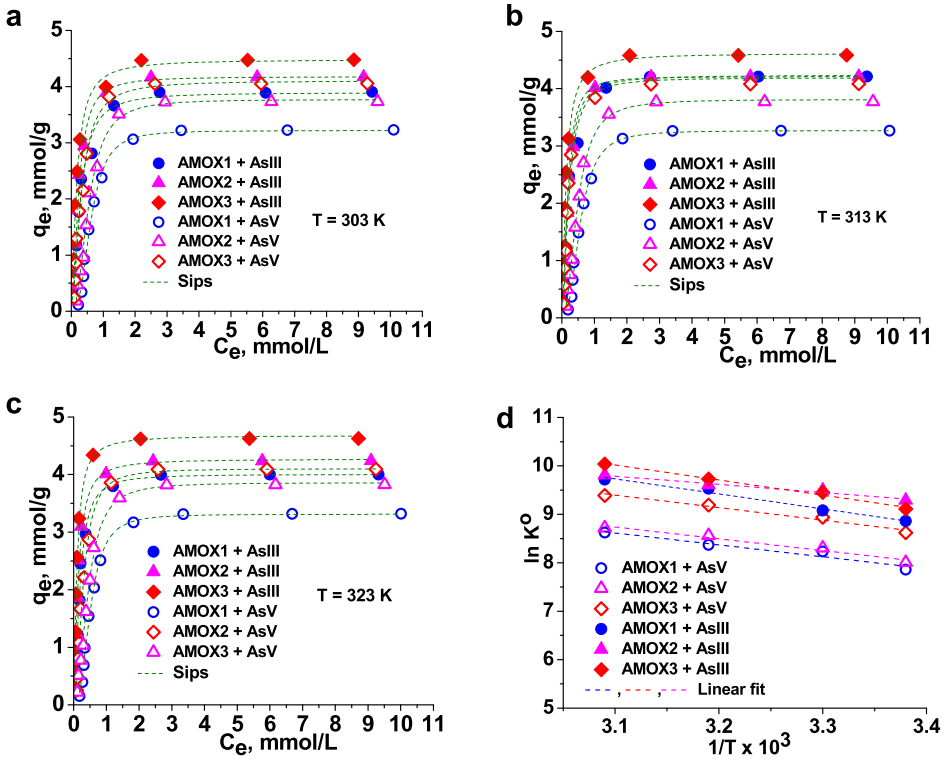

Figure 5. (a, b, c) Experimental sorption isotherms for the adsorption of As(III) and As(V) fitted by Sips isotherm. (d) Plot of ln K^{o} vs $1/T$ for the sorption of As(III) and arsenate oxyanions onto AMOX sorbents.

https://doi.org/10.1021/acsomega.2c03140
ACS Omega 2022, 7, 31069−31080

Table 4. Thermodynamic Parameters for the Adsorption of As(III) onto AMOX Sorbents

	$\Delta H°$, kJ mol^{-1}	$\Delta S°$, J mol^{-1} K^{-1}	$\Delta G°$, kJ mol^{-1}			
sorbent			295	303	313	323
AMOX1	25.75	160	−21.73	−22.77	−24.8	−26.1
AMOX2	13.97	124	−22.78	−23.93	−24.99	−26.34
AMOX3	25.89	163	−22.34	−23.81	−25.32	−26.96

Table 5. Thermodynamic Parameters for the Adsorption of As(V) Oxoanions

			$\Delta G°$, kJ mol^{-1}			
sorbent	$\Delta H°$, kJ mol^{-1}	$\Delta S°$, J mol^{-1} K^{-1}	295	303	313	323
AMOX1	20.43	134	−19.27	−20.74	−21.78	−23.16
AMOX2	20.20	135	−19.63	−20.92	−22.27	−23.42
AMOX3	21.52	144	−21.14	−22.52	−23.91	−25.22

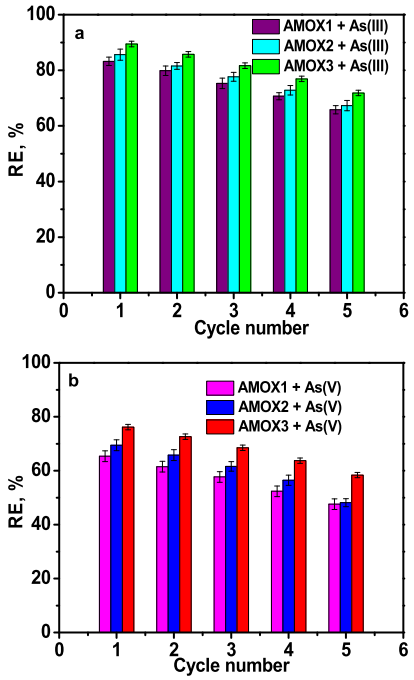

Figure 6. Reusability of AMOX composites in the removal of As(III) (a) and As(V) (b) as a function of sorption/desorption cycle number: sorption conditions: sorbent dose 1 g/L, pH 8, for As(III), and pH 5 for As(V), temperature 22 °C, contact time 8 h; desorption conditions: elution with 0.2 M HCl (8 h), regeneration with 0.1 M NaOH (6 h).

4. CONCLUSIONS

Composite sorbents consisting of amidoxime resin entrapped into the pores of a mesoporous silica were prepared and tested for their performances in the removal of As(III) and As(V) as a function of the amidoxime content and textural characteristics of the composites. The removal capacity of AMOX composites toward As(III) and As(V) from water was found to be strongly dependent on the initial pH (the optimum pH for the removal of As(V) was 5.0, while for As(III), the optimum pH was 8.0), initial concentration of arsenic anions, and the presence of interfering anions. The adsorption mechanism was the most probable physisorption, as indicated by the sorption kinetics (fitted the best by the PFO kinetic model), and by the values of the mean free energy of adsorption (E), whose values were 10−12 kJ/mol. Among the competitive anions, sulfate ions had moderate adverse effects, while the most significant interference occurred in the presence of phosphate and bicarbonate anions. The AMOX sorbents could be regenerated and reused up to five cycles, with an average loss of the RE of about 18%, for both arsenic species. The main advantage of the AMOX sorbents investigated in the present study is their applicability for the removal of both As(III) and As(V), being well known that usually As(III) and As(V) co-exist in groundwater.

■ ASSOCIATED CONTENT

Supporting Information

The Supporting Information is available free of charge at https://pubs.acs.org/doi/10.1021/acsomega.2c03140.

TG (a) and DTG (b) curves of the AMOX composite sorbents; pore size distribution for AMOX composites; experimental isotherms of As(III) and As(V) adsorption onto AMOX composite sorbents fitted by the Dubinin−Radushkevich isotherm model; and kinetic parameters for the adsorption of As(III) And As(V) onto AMOX composite sorbents (PDF)

■ AUTHOR INFORMATION

Corresponding Author

Ecaterina Stela Dragan − *"Petru Poni" Institute of Macromolecular Chemistry, Iasi 700487, Romania;* orcid.org/0000-0003-3656-6754; Phone: +40 232 217454; Email: sdragan@icmpp.ro; Fax: +40 232 211299

Authors

Doina Humelnicu − *Faculty of Chemistry, "Al. I. Cuza" University of Iasi, Iasi 700506, Romania*

Maria Ignat − *Faculty of Chemistry, "Al. I. Cuza" University of Iasi, Iasi 700506, Romania; "Petru Poni" Institute of Macromolecular Chemistry, Iasi 700487, Romania*

Maria Valentina Dinu − *"Petru Poni" Institute of Macromolecular Chemistry, Iasi 700487, Romania*

Complete contact information is available at: https://pubs.acs.org/10.1021/acsomega.2c03140

Notes

The authors declare no competing financial interest.

■ ACKNOWLEDGMENTS

The authors are grateful to the Romanian Academy for the support in the elaboration of this article.

REFERENCES

(1) Hao, L.; Liu, M.; Wang, N.; Li, G. A Critical Review on Arsenic Removal from Water Using Iron-Based Adsorbents. *RSC Adv.* **2018**, *8*, 39545−39560.

(2) Maia, L. C.; Soares, L. C.; Alves Gurgel, L. V. A. A Review on the Use of Lignocellulosic Materials for Arsenic Adsorption. *J. Environ. Manage.* **2021**, *288*, 112397.

(3) Rathi, B. S.; Kumar, P. S. A Review on Sources, Identification and Treatment Strategies for the Removal of Toxic Arsenic from Water System. *J. Hazard. Mater.* **2021**, *418*, 126299.

(4) Yao, R.; Yang, H. An Overview on As(V) Removal from Water by Adsorption Technology. *Ann. Muscoskel. Med.* **2020**, *4*, 015−020.

(5) Ha, H. N. N.; Phuong, N. T. K.; An, T. B.; Tho, T. M.; Thang, T. N.; Minh, B. Q.; Du, C. V. Arsenate Removal by Layered Double Hydroxides Embedded into Spherical Polymer Beads: Batch and Column Studies. *J. Environ. Sci. Health, Part A: Environ. Sci. Eng.* **2016**, *51*, 403−413.

(6) Mohan, D.; Pittman, C. U., Jr. Arsenic Removal from Water/Wastewater Using Adsorbents - A Critical Review. *J. Hazard. Mater.* **2007**, *142*, 1−53.

(7) Sharma, S.; Balasubramanian, K.; Arora, R. Adsorption of Arsenic(V) Ions onto Cellulosic-Ferric Oxide System: Kinetics and Isotherm Studies. *Desalin. Water Treat.* **2015**, *57*, 9420−9436.

(8) Karakurt, S.; Pehlivan, E.; Karakurt, S. Removal of Carcinogenic Arsenic from Drinking Water by the Application of Ion Exchange Resins. *Oncogen* **2019**, *2*, 1−8.

(9) Weerasundara, L.; Ok, Y. S.; Bundschuh, J. Selective Removal of Arsenic in Water: A Critical Review. *Environ. Pollut.* **2021**, *268*, 115668.

(10) Elcik, H.; Celik, S. O.; Cakmakci, M.; Özkaya, B. Performance of Nanofiltration and Reverse Osmosis Membranes for Arsenic Removal from Drinking Water. *Desalin. Water Treat.* **2016**, *57*, 20422−20429.

(11) Nidheesh, P. V.; Singh, T. S. Arsenic Removal by Electrocoagulation Process: Recent Trends and Removal Mechanism. *Chemosphere* **2017**, *181*, 418−432.

(12) Li, Y.; Qi, X.; Li, G.; Wang, H. Double-Pathway Arsenic Removal and Immobilization from High Arsenic-Bearing Wastewater by Using Nature Pyrite as in situ Fe and S Donator. *Chem. Eng. J.* **2021**, *410*, 128303.

(13) Çermikli, E.; Şen, F.; Altıok, E.; Wolska, J.; Cyganowski, P.; Kabay, N.; Bryjak, M.; Arda, M.; Yüksel, M. Performances of Novel Chelating Ion Exchange Resins for Boron and Arsenic Removal from Saline Geothermal Water Using Adsorption-Membrane Filtration Hybrid Process. *Desalination* **2020**, *491*, 114504.

(14) Chiavola, A.; D'Amato, E.; Gavasci, R.; Sirini, P. Arsenic Removal from Groundwater by Ion Exchange and Adsorption Processes: Comparison of Two Different Materials. *Water Sci. Technol.: Water Supply* **2015**, *15*, 981−989.

(15) de Namor, A. F.; Hakawati, A. A.; Hamdan, W. A.; Soualhi, R.; Korfali, S.; Valiente, L. Calix[4]Pyrrole for the Removal of Arsenic (III) and Arsenic (V) from Water. *J. Hazard. Mater.* **2017**, *326*, 61−68.

(16) Dudek, S.; Kołodyńska, D. Arsenate Removal on the Iron Oxide Ion Exchanger Modified with Neodynium(III) Ions. *J. Environ. Manage.* **2022**, *307*, 114551.

(17) Hubicki, Z.; Koodynsk, D. Selective removal of heavy metal ions from water and waste waters using ion exchange methods. *Ion Exchange Technologies*; Intechopen, 2012; pp 193−240.

(18) Zhang, Q.; Pan, B.; Zhang, W.; Pan, B.; Zhang, Q.; Ren, H. Arsenate Removal from Aqueous Media by Nanosized Hydrated Ferric Oxide (HFO)-Loaded Polymeric Sorbents: Effect of HFO Loadings. *Ind. Eng. Chem. Res.* **2008**, *47*, 3957−3962.

(19) Dax, D.; Chávez, M. S.; Xu, C.; Willför, S.; Mendonça, R. T.; Sánchez, J. Cationic Hemicellulose-Based Hydrogels for Arsenic and Chromium Removal from Aqueous Solutions. *Carbohydr. Polym.* **2014**, *111*, 797−805.

(20) Rios-Saldaña, L. E.; Pérez-Rodríguez, F.; Vence-Alvarez, E.; Nieto-Delgado, C.; Rangel-Mendez, J. R. Synthesis of a Granular Composite Based on Polyvinyl Alcohol-Fe:Ce Bimetallic Oxide Particles for the Selective Adsorption of As(V) from Water. *J. Water Proc. Eng.* **2022**, *46*, 102621.

(21) Du, Y.; Qiu, S.; Zhang, X.; Nie, G. Nanoconfined Hydrous Titanium Oxides with Excellent Acid Stability for Selective and Efficient Removal of As(V) from Acidic Wastewater. *Chem. Eng. J.* **2020**, *400*, 125907.

(22) Li, H.; Shan, C.; Zhang, Y.; Cai, J.; Zhang, W.; Pan, B. Arsenate Adsorption by Hydrous Ferric Oxide Nanoparticles Embedded in Cross-Linked Anion Exchanger: Effect of the Host Pore Structure. *ACS Appl. Mater. Interfaces* **2016**, *8*, 3012−3020.

(23) Saiz, J.; Bringas, E.; Ortiz, I. New Functionalized Magnetic Materials for As^{5+} Removal: Adsorbent Regeneration and Reuse. *Ind. Eng. Chem. Res.* **2014**, *53*, 18928−18934.

(24) Angotzi, M. S.; Mameli, V.; Cara, C.; Borchert, K. B. L.; Steinbach, C.; Boldt, R.; Schwarz, D.; Cannas, C. Meso- and Macroporous Silica-Based Arsenic Adsorbents: Effect of Pore Size, Nature of the Active Phase, and Silicon Release. *Nanoscale Adv.* **2021**, *3*, 6100−6113.

(25) Dobrynska, J. Amine- and Thiol-Functionalized SBA-15: Potential Materials for As(V), Cr(VI) And Se(VI) Removal from Water. Comparative Study. *J. Water Proc. Eng.* **2021**, *40*, 101942.

(26) Fan, H. T.; Fan, X.; Li, J.; Guo, M.; Zhang, D.; Yan, F.; Sun, T. Selective Removal of Arsenic(V) from Aqueous Solution Using a Surface-Ion Imprinted Amine-Functionalized Silica Gel Sorbent. *Ind. Eng. Chem. Res.* **2012**, *51*, 5216−5223.

(27) Liu, P.; Liang, Q.; Luo, H.; Fang, W.; Geng, J. Synthesis of Nano-Scale Zero-Valent Iron-Reduced Graphene Oxide-Silica Nano-Composites for the Efficient Removal of Arsenic from Aqueous Solutions. *Environ. Sci. Pollut. Res.* **2019**, *26*, 33507−33516.

(28) Valdés, O.; Marican, A.; Mirabal-Gallardo, Y.; Santos, L. S. Selective and Efficient Arsenic Recovery From Water Through Quaternary Amino-Functionalized Silica. *Polymers* **2018**, *10*, 626.

(29) Dragan, E. S.; Bucatariu, F. Design and Characterization of Anionic Hydrogels Confined in Daisogel Silica Composite Microspheres and Their Application in Sustained Release of Proteins. *Colloids Surf., A* **2016**, *489*, 46−56.

(30) Dragan, E. S.; Dinu, M. V. Spectacular Selectivity in the Capture of Methyl Orange by Composite Anion Exchangers with the Organic Part Hosted by Daisogel Microspheres. *ACS Appl. Mater. Interfaces* **2018**, *10*, 20499−20511.

(31) Dragan, E. S.; Humelnicu, D.; Ignat, M.; Varganici, C. D. Superadsorbents for Strontium and Cesium Removal Enriched in Amidoxime by a Homo-IPN Strategy Connected with Porous Silica Texture. *ACS Appl. Mater. Interfaces* **2020**, *12*, 44622−44638.

(32) Lu, S.; Chen, L.; Hamza, M. F.; He, C.; Wang, X.; Wei, Y.; Guibal, E. Amidoxime Functionalization of a Poly(Acrylonitrile)/Silica Composite for the Sorption of Ga(III) − Application to the Treatment of Bayer Liquor. *Chem. Eng. J.* **2019**, *368*, 459−473.

(33) Elwakeel, K. Z.; El-Bindary, A. A.; Kouta, E. Y.; Guibal, E. Functionalization of Polyacrylonitrile/Na-Y-Zeolite Composite with Amidoxime Groups for the Sorption of Cu(II), Cd(II) and Pb(II) Metal Ions. *Chem. Eng. J.* **2018**, *332*, 727−736.

(34) Alexandratos, S. D.; Zhu, X.; Florent, M.; Sellin, R. Polymer-Supported Bifunctional Amidoximes for the Sorption of Uranium from Seawater. *Ind. Eng. Chem. Res.* **2016**, *55*, 4208−4216.

(35) Hanh, T. T.; Huy, H. T.; Hien, N. Q. Pre-irradiation Grafting of Acrylonitrile onto Chitin for Adsorption of Arsenic in Water. *Radiat. Phys. Chem.* **2015**, *106*, 235−241.

(36) Dragan, E. S. Advances in Interpenetrating Polymer Network Hydrogels and Their Applications. *Pure Appl. Chem.* **2014**, *86*, 1707−1721.

(37) Corazzari, I.; Nisticò, R.; Turci, F.; Faga, M. G.; Franzoso, F.; Tabasso, S.; Magnacca, M. Advanced Physico-Chemical Characterization of Chitosan by Means of TGA Coupled On-Line with FTIR and GCMS: Thermal Degradation and Water Adsorption Capacity. *Polym. Degrad. Stab.* **2015**, *112*, 1−9.

(38) Hong, H. J.; Kim, B. G.; Ryu, J.; Park, I. S.; Chung, K. S.; Lee, S. M.; Lee, J. B.; Jeong, H. S.; Kim, H.; Ryu, T. Preparation of Highly Stable Zeolite-Alginate Foam Composite for Strontium (^{90}Sr) Removal from Seawater and Evaluation of Sr Adsorption Performance. *J. Environ. Manage.* **2018**, *205*, 192−200.

https://doi.org/10.1021/acsomega.2c03140
ACS Omega 2022, 7, 31069−31080

(39) Ozkula, G.; Urbano, B. F.; Rivas, B. L.; Kabay, N.; Bryjak, M. Arsenic Sorption Using Mixtures of Ion Exchange Resins Containing N-Methyl-D-Glucamine and Quaternary Ammonium Groups. *J. Chil. Chem. Soc.* **2016**, *61*, 2752−2756.
(40) Boddu, V. M.; Abburi, K.; Talbott, J. L.; Smith, E. D.; Haasch, R. Removal of Arsenic (III) and Arsenic (V) from Aqueous Medium Using Chitosan-Coated Biosorbent. *Water Res.* **2008**, *42*, 633−642.
(41) Lee, C. G.; Alvarez, P. J. J.; Nam, A.; Park, S. J.; Do, T.; Choi, U.; Lee, S. Arsenic(V) Removal Using an Amine-Doped Acrylic Ion Exchange Fiber: Kinetic, Equilibrium, and Regeneration Studies. *J. Hazard. Mater.* **2017**, *325*, 223−229.
(42) Yu, X.; Tong, S.; Ge, M.; Wu, L.; Zuo, J.; Cao, C.; Song, W. Synthesis and Characterization of Multi-Amino-Functionalized Cellulose for Arsenic Adsorption. *Carbohydr. Polym.* **2013**, *92*, 380−387.
(43) Raychoudhury, T.; Schiperski, F.; Scheytt, T. Distribution of Iron in Activated Carbon Composites: Assessment of Arsenic Removal Behavior. *Water Sci. Technol.: Water Supply* **2015**, *15*, 990−998.
(44) Wei, J.; Shen, B.; Ye, G.; Wen, X.; Song, Y.; Wang, J.; Meng, X. Selenium and Arsenic Removal from Water Using Amine Sorbent, Competitive Adsorption and Regeneration. *Environ. Pollut.* **2021**, *274*, 115866.
(45) Kumar, M.; Mukherjee, S.; Thakur, A. K.; Raval, N.; An, A.; Gikas, P. Aminoalkyl-organo-silane Treated Sand for the Adsorptive Removal of Arsenic from the Groundwater: Immobilizing the Mobilized Geogenic Contaminants. *J. Hazard. Mater.* **2022**, *425*, 127916.
(46) Lagergren, S. Zur Theorie Der Sogenannten Adsorption Geloster Stoffe. *K. Sven. Vetenskapsakad. Handl.* **1898**, *24*, 1−39.
(47) Ho, Y. S.; Mckay, G. The Kinetics of Sorption of Basic Dyes from Aqueous Solution by Sphagnum Moss Peat. *Can. J. Chem. Eng.* **1998**, *76*, 822−827.
(48) Juang, R. S.; Chen, M. L. Application of the Elovich Equation to the Kinetics of Metal Sorption with Solvent-Impregnated Resins. *Ind. Eng. Chem. Res.* **1997**, *36*, 813−820.
(49) Weber, J. W. J.; Morris, J. C. Kinetics of Adsorption on Carbon from Solution. *J. Sanit. Eng. Div., Am. Soc. Civ. Eng.* **1963**, *89*, 31−59.
(50) Ayawei, N.; Ebelegi, A. N.; Wankasi, D. Modelling and Interpretation of Adsorption Isotherms. Review Article. *J. Chem.* **2017**, *2017*, 3039817.
(51) Foo, K. Y.; Hameed, B. H. Insights into the Modeling of Adsorption Isotherm Systems. *Chem. Eng. J.* **2010**, *156*, 2−10.
(52) Dragan, E. S.; Humelnicu, D.; Dinu, M. V. Designing Smart Triple-Network Cationic Cryogels with Outstanding Efficiency and Selectivity for Deep Cleaning of Phosphate. *Chem. Eng. J.* **2021**, *426*, 131411.
(53) Humelnicu, D.; Lazar, M. M.; Ignat, M.; Dinu, I. A.; Dragan, E. S.; Dinu, M. V. Removal of Heavy Metal Ions from Multi-Component Aqueous Solutions by Eco-Friendly and Low-Cost Composite Sorbents with Anisotropic Pores. *J. Hazard. Mater.* **2020**, *381*, 120980.
(54) Vieira, T.; Artifon, S. E. S.; Cesco, C. T.; Vilela, P. B.; Becegato, V. A.; Paulino, A. T. Chitosan-based Hydrogels for the Sorption of Metals and Dyes in Water: Isothermal, Kinetic, and Thermodynamic Evaluations. *Colloid Polym. Sci.* **2021**, *299*, 649−662.
(55) Zhou, X. Correction to the Calculation of Polanyi Potential from Dubinin-Radushkevich Equation. *J. Hazard. Mater.* **2020**, *384*, 121101.
(56) Puccia, V.; Avena, M. J. On the Use of the Dubinin-Radushkevich Equation to Distinguish between Physical and Chemical Adsorption at the Solid-Water Interface. *Colloid Interface Sci. Commun.* **2021**, *41*, 100376.
(57) Neiber, R. R.; Galhoum, A. A.; El Sayed, I. E. T.; Guibal, E.; Xin, J.; Lu, X. Selective Lead (II) Sorption Using Aminophosphonate-Based Sorbents: Effect of Amine Linker, Characterization and Sorption Performance. *Chem. Eng. J.* **2022**, *442*, 136300.
(58) Gupta, A.; Chauhan, V. S.; Sankararamakrishnan, N. Bimetallic Fe/Ni Nanoparticles Derived from Green Synthesis for the Removal of Arsenic (V) in Mine Wastewater. Preparation and Evaluation of Iron−Chitosan Composites for Removal of As(III) and As(V) from Arsenic Contaminated Real Life Groundwater. *Water Res.* **2009**, *43*, 3862−3870.
(59) Kailasam, V.; Rosenberg, E.; Nielsen, D. Characterization of Surface-Bound Zr(IV) and Its Application to Removal of As(V) and As(III) from Aqueous Systems Using Phosphonic Acid Modified Nanoporous Silica Polyamine Composites. *Ind. Eng. Chem. Res.* **2009**, *48*, 3991−4001.
(60) Ouyang, L.; Wang, Y.; Zhang, P.; Wang, X.; Yuan, S. Heterostructured MWCNTs@ PANI@TiO2 Nanocomposites for Enhanced Adsorption of As(III) from Aqueous Solution: Adsorption and Photocatalytic Oxidation Behaviors. *Ind. Eng. Chem. Res.* **2020**, *59*, 11743−11756.
(61) Lin, Y.; Jin, X.; Khan, N. I.; Owens, G.; Chen, Z. Bimetallic Fe/Ni Nanoparticles Derived From Green Synthesis for the Removal of Arsenic (V) in Mine Wastewater. *J. Environ. Manage.* **2022**, *301*, 113838.
(62) Tchieda, V. K.; D'Amato, E.; Chiavola, A.; Parisi, M.; Chianese, A.; Amamra, M.; Kanaev, A. Removal of Arsenic by Alumina: Effects of Material Size, Additives, and Water Contaminants. *Clean: Soil, Air, Water* **2016**, *44*, 496−505.
(63) Yin, L.; Liu, L.; Lin, S.; Owens, G.; Chen, Z. Synthesis and Characterization of Nanoscale Zero-Valent Iron (nZVI) as an Adsorbent for the Simultaneous Removal of As(III) and As(V) from Groundwater. *J. Water Proc. Eng.* **2022**, *47*, 102677.
(64) Gao, X.; Wang, Y.; Hu, Q.; Su, C. Effects of Anion Competitive Adsorption on Arsenic Enrichment in Groundwater. *J. Environ. Sci. Health, Part A: Environ. Sci. Eng.* **2011**, *46*, 471−479.
(65) Myneni, S.; Traina, S. J.; Waychunas, G. A.; Logan, T. J. Experimental and Theoretical Vibrational Spectroscopic Evaluation of Arsenate Coordination in Aqueous Solutions, Solids, and at Mineral-Water Interfaces. *Geochim. Cosmochim. Acta* **1998**, *62*, 3285−3300.
(66) Tran, H. N.; Lima, E. C.; Juang, R. S.; Bollinger, J. C.; Chao, H. P. Thermodynamic Parameters of Liquid-Phase Adsorption Process Calculated from Different Equilibrium Constants Related to Adsorption Isotherms: A Comparison Study. *J. Environ. Chem. Eng.* **2021**, *9*, 106674.

https://doi.org/10.1021/acsomega.2c03140
ACS Omega 2022, 7, 31069−31080